

Pitting corrosion studies of super austenitic stainless steels in natural sea water using dynamic electrochemical impedance spectroscopy

S. NAGARAJAN, M. KARTHEGA and N. RAJENDRAN*

Department of Applied Sciences and Humanities, MIT Campus, Anna University, Chromepet, Chennai, 600 044, India
(*author for correspondence, e-mail: nrajendran@annauniv.edu)

Received 22 November 2005; accepted in revised form 11 August 2006

Key words: DEIS, pitting corrosion, polarisation studies, super austenitic stainless steel

Abstract

Potentiodynamic anodic polarisation and dynamic electrochemical impedance spectroscopic (DEIS) measurements were carried out on type 316L stainless steel (SS), alloys 33 and 24 in natural sea water environment in order to assess pitting corrosion resistance. The results revealed that the pitting corrosion resistance was higher in the case of alloys 33 and 24 than 316L SS; due to the higher contents of nitrogen, chromium and molybdenum. DEIS measurements were performed over a wide range of potentials covering the corrosion potential, passive region, breakdown region and dissolution region. It was shown that the impedance measurements in potentiodynamic conditions allow simultaneous investigation of changes in passive layer structure. The impedance spectra of various potential regions were also discussed. The Nyquist plots were fitted using non-linear least-square (NLSS) method for different potential regions.

1. Introduction

Stainless steel (SS) shows excellent resistance to corrosion in various environments due to the formation of a highly protective surface film. However, in many cases, particularly in the presence of chlorides, SS undergoes localised attack, resulting in pitting, crevice corrosion and stress corrosion cracking. Studies on corrosion resistance of SS in natural and synthetic sea water showed that the SS were corroded by natural sea water at rates of one order of magnitude higher than by synthetic sea water [1, 2]. These attacks of chloride ions lead to corrosion, which are associated with the localised break down of the surface passive film. In order to circumvent these problems, the passive nature has to be tuned for better resistance to pitting. To achieve this, attempts have been made to change to composition of the alloys with suitable elements, which improve the life expectancy of the materials used for demanding applications. In general, elements such as chromium, nickel, molybdenum and nitrogen are added in various ratios to provide an improved corrosion resistance [3–7]. The effective applications of high alloy SS in the marine environment, which are particularly pertinent to desalination, have been reviewed in a number of articles [8–10]. Development of new alloys required evaluation related to their ability of surviving against pitting corrosion in any

aggressive medium. This is generally carried out through electrochemical techniques.

Although various electrochemical techniques are used for characterising the localised corrosion behaviour, Electrochemical Impedance Spectroscopy (EIS) has outclassed other techniques for testing the phenomena that take place in a metal/solution interface in the electrochemical system. EIS was employed to detect and monitor pitting corrosion of various materials such as Al and its alloys, stainless steels, Fe–Cr alloys [11–16]. Oltra and Keddam [17, 18] compared the impedance data with a theoretical model of pitting corrosion and pointed out the non-steady character of the corrosion process, mainly during the initiation and development of pits.

Recently, Darowicki et al. [19–21] developed a new impedance method termed dynamic electrochemical impedance spectroscopy (DEIS). This method of impedance, essentially carried out under potentiodynamic conditions, have the capability to record the impedance spectra at the point of pitting corrosion. Also, this completely novel and versatile method creates new investigational possibilities.

In the present work, the DEIS has been exploited to study the corrosion behaviour of 316L SS and super austenitic stainless steels viz., alloys 33 and 24. The impedance spectra obtained due to the response of the passive film under various applied over-voltages have been studied

Table 1. Chemical composition of investigated alloys (wt.%).

Alloy	Main alloying elements/wt. %					
	Cr	Ni	Mo	N	C	Mn
316L SS	17.2	12.60	2.40	0.02	0.03	1.950
Alloy 33	24.2	30.95	1.67	0.39	0.01	0.004
Alloy 24	32.9	17.70	4.34	0.19	0.01	6.140

2. Experimental procedure

The chemical compositions of the 316L SS, alloys 33 and 24 are given in Table 1. The specimens were cut in the dimension of $10 \times 10 \times 3$ mm and were attached using a brass rod for electrical connection. Then they were moulded with an epoxy-based resin. The exposed surface area was 1 cm^2 and was polished using abrasive SiC paper up to 1200 grade and final polishing was done using 1μ diamond paste in order to obtain a scratch free mirror finish. This was followed by rinsing with distilled water and subsequently degreasing with acetone.

A conventional three electrode cell was used for all the electrochemical measurements. A saturated calomel electrode (SCE) was used as a reference electrode, platinum foil as a counter electrode and the test material as a working electrode. Natural sea water collected from the coastal area of Chennai, India served as the electrolyte.

Potentiodynamic cyclic polarisation studies were carried out for the test specimens in natural sea water. The potentiostat (model PGSTAT 12, AUTOLAB, the Netherlands B.V.) controlled by a personal computer with dedicated software (GPES Version 4.9.005) was used for conducting the polarisation experiments. The potential was applied on the working electrode at a scan rate of 0.167 mV s^{-1} from open circuit potential. The sweep direction was reversed at a current density of 3 mA cm^{-2} and scanning was continued till the potential at which the current density in the forward scan was equal to that in the reverse scan. In order to test the reproducibility, the experiments were repeated thrice.

DEIS measurements were carried out using a Frequency Response Analyser (FRA), which included a potentiostat model PGSTAT 12. Impedance spectra were acquired from the corrosion potential till the dissolution region in the frequency range of $55 \text{ kHz} - 0.1 \text{ Hz}$ with a 10 mV amplitude sine wave generated by a frequency response analyzer. The potentials were increased with a step potential of 20 mV . The spectra were interpreted using the non-linear least-square fitting procedure developed by Boukamp [22].

3. Results and discussion

3.1. Potentiodynamic anodic polarisation

Figure 1 shows the potentiodynamic anodic cyclic polarisation curves of reference type 316L SS, alloys

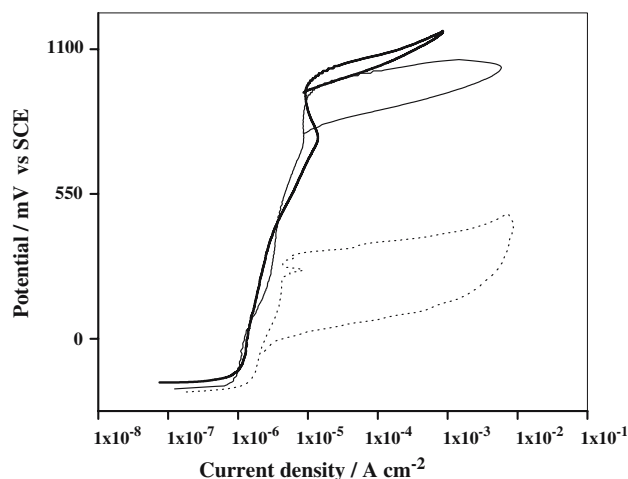


Fig. 1. Potentiodynamic cyclic polarisation curves for (.....) 316L SS, (---) alloy 33 and (—) alloy 24 in natural sea water.

33 and 24 in natural sea water. The critical pitting potentials (E_b) for alloys 33 and 24 were 989 mV and 1034 mV , respectively, whereas for the reference material the potential was 310 mV . The values indicate that alloys 33 and 24 exhibit a higher pitting resistance in natural sea water.

The pit repassivation potential (E_p) was determined for the above alloys from the polarisation curves (Figure 1). The repassivation potential for the type 316L SS was found to be -138 mV , whereas for alloys 33 and 24, it was 757 mV and 912 mV , respectively.

The difference between the critical pitting potential (E_b) and the pit repassivation potential (E_p) for a given system is defined as the relative corrosion resistance ($\Delta E = E_b - E_p$). The magnitude of ΔE is often considered as an indicator of pitting resistance, that is, the higher the ΔE value, the lower the pitting resistance of the material [23]. This value can be used to rank the alloys [24]. The mean value of ΔE for 316L SS was found to be 451 mV , whereas alloys 33 and 24 showed lower ΔE values of 232 mV and 122 mV , respectively. Thus the lower ΔE values for alloys 33 and 24 reflect the enhanced pitting corrosion resistance.

The area of the hysteresis loop is a direct measure of the pit propagation kinetics. A large hysteresis loop was observed for 316L SS, whereas for alloys 33 and 24, the loop obtained was small. This indicates that the 316L SS is susceptible to pitting corrosion in natural sea water, whereas alloys 33 and 24 show better corrosion resistance.

The significance of these observations shows an enhanced pitting corrosion resistance of alloys 33 and 24, compared with 316L SS. This behaviour can be attributed to the higher amounts of alloying elements, namely, nickel, chromium, molybdenum and nitrogen in alloys 33 and 24. In the case of super austenitic alloys, if a pit grows in the austenitic phase, the conditions prevailing at that pit site have been reported to be similar to those of the active dissolution state. During

active dissolution, nickel and chromium generally dissolve, whereas non-active elements such as nitrogen and molybdenum can enrich at the surface. Newman and Shahrabi [25] have reported the enrichment of molybdenum and nitrogen in the passive film/metal interface.

However, the mechanism involved in the pitting resistance of alloys 33 and 24 might be marginally different because of the compositional variation. Alloy 33, which has higher nitrogen content, might possess a passive film enriched in nitrogen. Reports claim that the nitrogen level in the passive film is seven times higher when compared with the original concentration [26, 27]. Moreover, the nitrogen present in the SS stabilises the austenitic phase and inhibits the anodic dissolution of the material at least by two orders of magnitude, presumably through the formation of iron nitride. This inhibits the autocatalytic process of pit formation and increases the opportunity for pit healing.

The pitting resistance of alloy 24 can be attributed to the tandem effect due to the presence of molybdenum and nitrogen in the alloy. In addition to the effect of nitrogen in the passive film, it has been reported that molybdenum enriched passive film exhibits multiple properties in the bipolar model, where the passive film is divided into a negatively charged cation, selective outer layer, and a positively charged anion, selective inner layer. The negatively charged outer layer repels the ingress of the chloride ions and the positively charged

inner layer resists the dissolution of metal at the oxide/metal surface [28]. Hence, a synergistic effect of nitrogen and molybdenum plays a vital role in enhancing the pitting corrosion resistance of alloy 24.

3.2. Potentiodynamic impedance spectroscopic studies

Figure 2(a–c) is a three dimensional representation of all the impedance spectra of 316 L SS, alloys 33 and 24, obtained from the potentiodynamic impedance studies. The impedance spectrum was obtained for every 20 mV increase in the potential, beginning from OCP to the dissolution potential. A linear increase in the magnitude of impedance irrespective of the alloy was observed from OCP. In the case of 316L SS, the magnitude drops sharply after attaining a maximum impedance value at a potential of 220 mV. In the case of alloy 33, the magnitude of impedance attained a maximum value approximately at 110 mV and then gradually decreased till a potential of 500 mV. Beyond this potential, the impedance rapidly claims to attain a maximum at 690 mV. This maximum has an impedance value half to that of the initial maxima observed at 110 mV. From 690 mV, there was a sharp decrease in the magnitude of impedance till the dissolution potential. In the case of alloy 24, a similar behaviour was observed to that of alloy 33. The initial maximum was observed around 160 mV. But the decrease in the magnitude of impedance beyond the potential was much lower compared

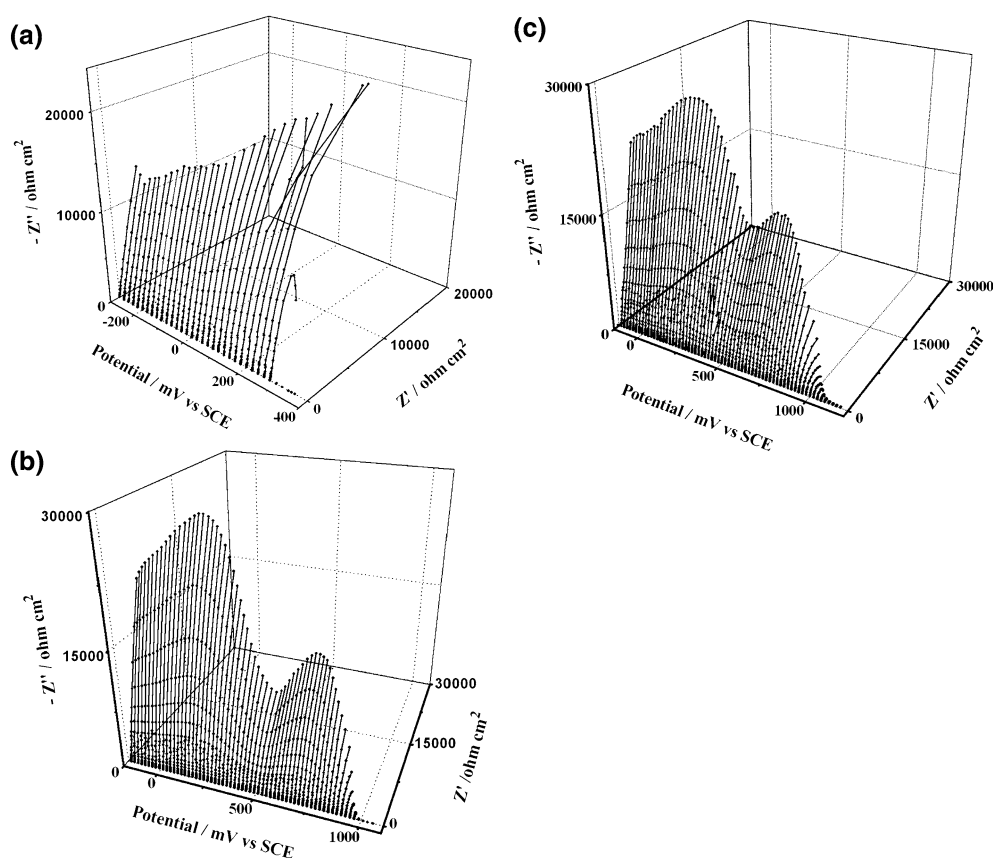


Fig. 2. The impedance versus potential diagram of (a) 316L SS (b) alloy 33 and (c) alloy 24.

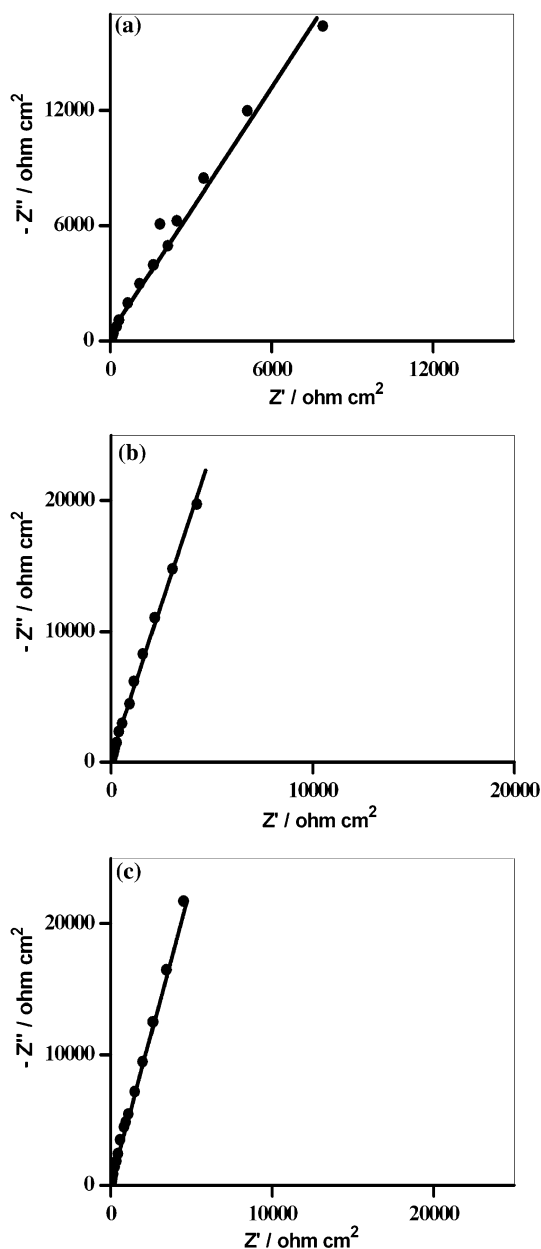


Fig. 3. Nyquist plot at open circuit potential for (a) 316L SS (b) alloy 33 and (c) alloy 24. Experimental (••) and calculated (—).

with alloy 33 and attained a minimum value around 500 mV. The secondary maximum was observed for alloy 24 at 700 mV before the gradual decline in the impedance value. The results obtained from DEIS, when correlated with polarisation curves of 316 L SS, alloys 33 and 24, revealed very minute details regarding the passive film behaviour starting from OCP till dissolution potential. For instance, firstly, all the alloys exhibited a maximum resistance before breakdown. Though polarisation curves also depicted the same, the result obtained from DEIS was more apparent. Secondly, in the case of alloys 33 and 24, the decline in the value before the secondary maxima, essentially due to the thinning of the passive film, was not clearly visible from the polarisation curves. Thirdly, the breakdown potentials can be determined precisely from DEIS.

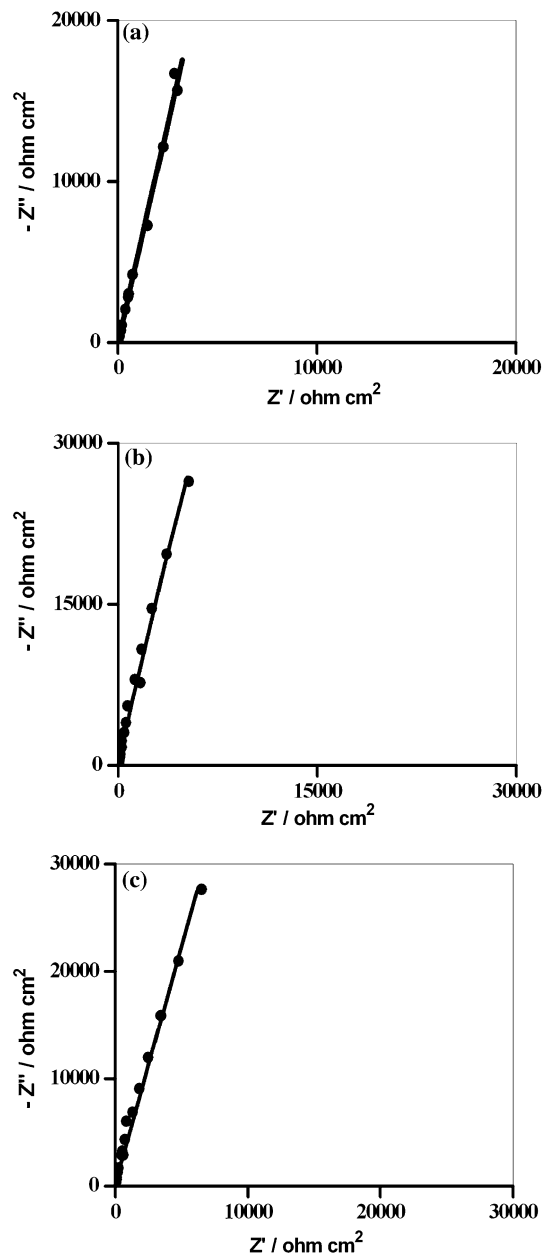


Fig. 4. Nyquist plot in passive region for (a) 316L SS (b) alloy 33 and (c) alloy 24. Experimental (••) and calculated (—).

In order to have a better understanding of the pitting process, electrochemical impedance spectra at a potential in each region, namely, OCP, passive, breakdown and dissolution were selected from the potentiodynamic electrochemical impedance spectra. Figures 3(a–d) and 4(a–d) represent the Nyquist plots at OCP and at a potential in the passive region for 316L SS, alloys 33 and 24, respectively. The spectra of all the alloys exhibited a similar behaviour containing a straight line with a high magnitude of impedance, which indicates a highly resistant passive film. Generally, the alloy surface is covered with continuous oxide film [29].

Figure 5(a–d) shows the impedance spectra of the alloys at the breakdown potential. The reference material 316L SS exhibited a semicircle with a low magnitude Warburg impedance at lower frequency. The Warburg

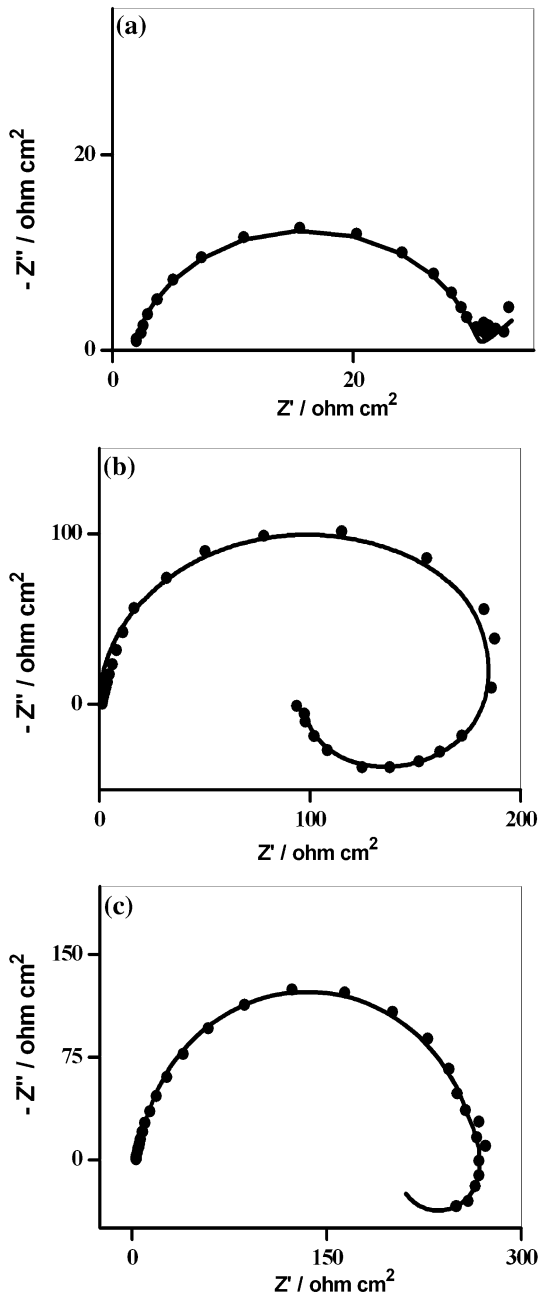


Fig. 5. Nyquist plot at breakdown potential for (a) 316L SS (b) alloy 33 and (c) alloy 24. Experimental (••) and calculated (—).

impedance observed can be attributed to a diffusion reaction taking place at the electrode surface. However, for alloys 33 and 24, a semicircle with a low magnitude inductive loop at lower frequency was observed.

The appearance of a capacitive loop in the form of a semicircle in alloys 33 and 24 can be due to a charge transfer at the film/solution interface. The inductive loop at lower frequency is most probably due to the relaxation process of an intermediate species of the dissolution reaction. Substantial reports are available for the presence of inductive loops in the low frequency range of the impedance spectra obtained for high alloys [30, 31].

Figure 6(a–d) shows the Nyquist plot of 316L SS, alloys 33 and 24 at dissolution region. The reference material, 316L SS, shows a semicircle, having lower impedance value with a more pronounced Warburg tail. The Nyquist plot corresponding to alloy 33 at the dissolution region exhibited an inductive loop similar to that of the spectra obtained at break down plot. However, the magnitude of the impedance was extremely low. Whereas, in the case of alloy 24, additional capacitive and inductive loops were observed apart from the loops obtained at the breakdown potential.

In the case of 316L SS, the Warburg impedance observed at and after breakdown potential may be

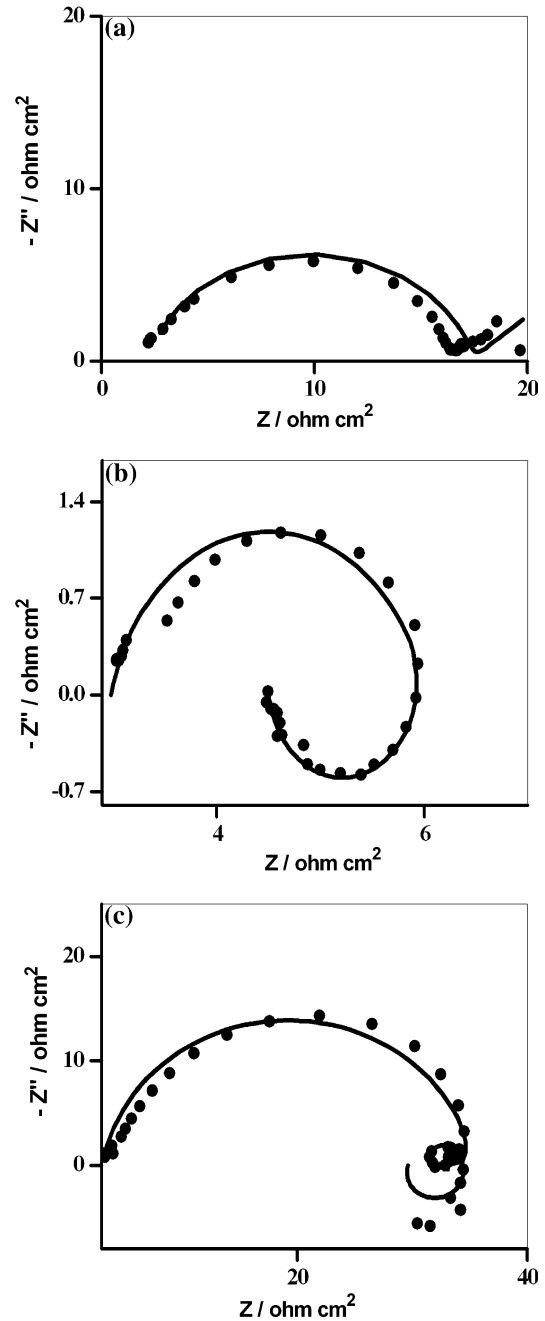


Fig. 6. Nyquist plot in dissolution region for (a) 316L SS (b) alloy 33 and (c) alloy 24. Experimental (••) and calculated (—).

attributed to an ionic diffusion through the solid corrosion products precipitated near the pit mouth as reported by Dawson and Ferreira [12]. In the case of alloy 33, the inductive loop at the low frequency region at and above the breakdown potential can be associated with the presence of an intermediate species. This intermediate species can be attributed to the enhanced pitting corrosion resistance of alloy 33. In the case of alloy 24, the inductive loop at the intermediate frequency may be due to the presence of an intermediate species at the film/solution interface. The following capacitive loop can be due to a time constant relaxation based on the adsorption/desorption process, and the second inductive loop may be due to a relaxation process which takes place at a slower phase. Generally, such slower relaxation processes do not play a significant role in the passivation behaviour.

The impedance data were fitted using equivalent circuits, each of the alloys exhibited a unique behaviour corresponding to the region of consideration. Hence, there were significant variations in the physical elements of the equivalent circuit among the alloys at various regions studied. In order to eliminate large errors, the data were fitted using various circuits and the best fit is represented in Figure 7(a–d).

Figure 7a represents the equivalent circuit model $R_s(R_1Q_1)$ used for fitting the impedance data for all the alloys in the OCP and passive regions, where, R_s , R_1 and Q_1 represent the solution resistance, the charge transfer resistance and double layer capacitance, respectively. The spectra obtained for 316L SS at the breakdown and dissolution regions were fitted using an equivalent circuit $R_s(Q_1(R_1W))$, where W represents the Warburg impedance. However, the spectra obtained at the breakdown region of alloys 33 and 24 were fitted using an equivalent circuit model $R_s(Q_1R_1[L_1R_2])$, as shown in Figure 7c. The same model was used for fitting the spectra at the dissolution region for alloy 33. Figure 7d represents the equivalent circuit model $R_s(Q_1R_1[L_1R_2][C_1R_3][L_2R_4])$ for fitting the impedance data of alloy 24 at the dissolution region. The equivalent circuit elements, namely, R_2, R_3, R_4, C_1, L_1 and L_2 involved in alloys 33 and 24 do not correspond physically to any passive electrical components as they have negative values [36]. Hence, these parameters are generally employed, only for an equivalent mathematical representation.

4. Conclusion

The relative corrosion resistance (ΔE) calculated for alloys 33 and 24 in natural sea water shows the higher pitting resistance, compared with 316L SS, which may be due to the presence of both nitrogen and molybdenum in the super austenitic alloys. The DEIS technique has been used to evaluate the pitting corrosion resistance of alloys 33 and 24 in natural sea water. The Nyquist plot at different potential regions, namely,

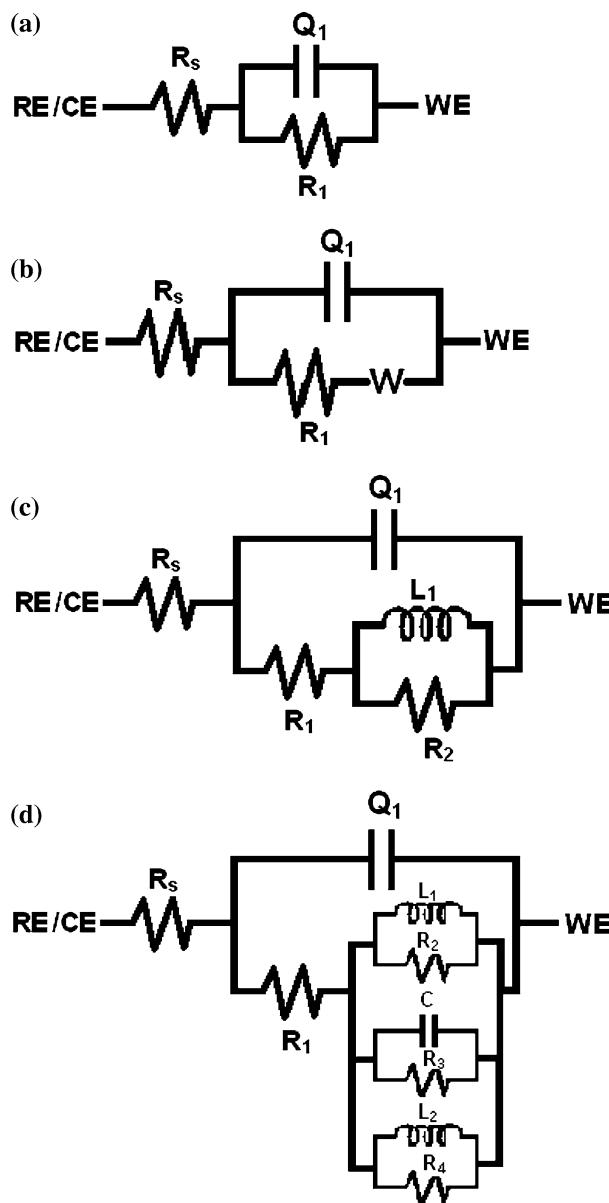


Fig. 7. Fitted equivalent circuit model for impedance data at different regions for all the alloys.

OCP, passive region, breakdown region and dissolution region reveals that the impedance changes as a function of potential. The critical pitting potential measured from the polarisation data is in good agreement with the dynamic electrochemical impedance spectroscopic data

References

1. T.S. Lee and K.L. Money, *Mater. Perform.* **24** (1984) 28.
2. P. Gallagher, R.E. Malpas and E.B. Shone, *Corrosion* **23** (1988) 229.
3. N. Rajendran and S. Rajeswari, *J. Mat. Sci.* **31** (1996) 6615.
4. N. Rajendran, G. Latha and S. Rajeswari, *Brit. Corros. J.* **37** (2002) 276.
5. R. Roth, *Workst. Korros.* **43** (1993) 275.
6. M.X. Cerney, *Corros. Rev.* **8** (1988) 60.
7. G. Mori and D. Bauernfeind, *Mater. and Corros.* **55** (2004) 164.

8. G. Latha, N. Rajendran and S. Rajeswari, Proceedings of the Fourth International Conference on Advance in Surface Engineering, May 1996 (Newcastle upon Tyne).
9. J.W. Oldfield and B. Tood, *Desalination* **108** (1996) 27.
10. A.V. Malik, S. Ahmad and S. Al-Fouzan, *Desalination* **97** (1994) 199.
11. F. Mansfeld and B. Little, *Corros. Sci.* **32** (1991) 247.
12. J.L. Dawson and M.G.S. Ferreira, *Corros. Sci.* **26** (1986) 1027.
13. T. Hong, G.W. Walter and M. Nagumo, *Corros. Sci.* **38** (1996) 1525.
14. P.Q. Zhang, J.X. Wu, W.Q. Zhang, X.Y. Lu and K. Wang, *Corros. Sci.* **33** (1993) 1343.
15. R.F.A. Jargolius-petterson and B.G. Pound, *J. Electrochem. Soc.* **145** (1998) 1462.
16. J. Galland, *Corros. Sci.* **39** (1997) 1239.
17. R. Oltra and M. Keddam, *Corros. Sci.* **28** (1988) 1.
18. R. Oltra and M. Keddam, *Electrochim. Act.* **35** (1990) 1619.
19. K. Darowicki, K. Krakowiak and P. Slepiski, *Electrochim. Act.* **49** (2004) 2909.
20. K. Krakowiak, K. Darowicki and P. Slepiski, *J. Electroanal. Chem.* **575** (2005) 33.
21. K. Krakowiak, K. Darowicki and P. Slepiski, *Electrochim. Act.* **50** (2005) 2699.
22. B.A. Boukamp, *Solid State Ionics* **21** (1986) 31.
23. D.A. Jones and B.E. Wilde, *Corros. Sci.* **18** (1978) 631.
24. M. Siva kumar, U. Kamchimudali and S. Rajeswari, *Steel Res.* **65** (1994) 79.
25. R.C. Newman and T. Shahrabi, *Corros. Sci.* **27** (1987) 827.
26. C.O.A. Ollson, *Corros. Sci.* **37** (1995) 467.
27. Y.C. Lu, C.R. Clayton and A.R. Brooks, *Corros. Sci.* **29** (1989) 863.
28. C.R. Clayton and Y.C. Lu, *J. Electrochem. Soc.* **133** (1986) 2465.
29. S. Masimovitch, *Electochim. Act.* **41** (1996) 2761.
30. S. Magaino, M. Matlosz and D. Landolt, *J. Electrochem. Soc.* **140** (1993) 1365.
31. I. Epelboin, C. Gabrielli, M. Keddam and H. Takenoçtli, *Electrochim. Act.* **20** (1975) 913.
32. R. Franceschetti and J.R. Macdonal, *J. Electroanal. Chem.* **82** (1977) 271.